Optimal Scale Selection for Circular Edge Extraction

Ji-Young Lim and H. Siegfried Stiehl

Universität Hamburg, Fachbereich Informatik, Arbeitsbereich Kognitive Systeme
Vogt-Kölln-Str. 30, 22527 Hamburg, Germany
{lim, stiehl}@informatik.uni-hamburg.de
http://kogs-www.informatik.uni-hamburg.de/~lim

Abstract. This paper addresses the issue of optimal scale selection for circular edge extraction in the context of higher dimensional multiscale edge extraction. Based on a classification of higher dimensional edges according to local curvature, we exemplarily establish a 2-D circular edge model. Through a careful mathematical derivation, we transform the circular edge model from Cartesian coordinates for which the analytical solution is unknown into polar coordinates. Utilizing this edge model we develop a novel theoretical framework for optimal scale selection for circular edge extraction through which the effects of curvature as related to scale can be analyzed. Moreover, we carry out a validation study in order to investigate on the level of principal performance how well the experimental results obtained from application of the developed framework to 2-D synthetic images match the theoretical results.

1 Introduction

Edge extraction is one of the key issues in image analysis and computer vision. The goal of edge extraction is to obtain a rich and meaningful description of an image by characterizing its intensity changes. Image intensity changes occur with many spatial scales depending on their physical origin. Only some of these stand out locally and seem to be more significant than others. Therefore, a natural requirement is to measure the local scale for each edge. This is the main motivation behind multiscale approaches to edge extraction on the basis of the linear scale-space theory (see e.g. [11]). A multiscale analysis for the purpose of coping with the problem associated with *fixed* scale approaches to edge extraction can reveal precious information about the nature of the underlying physical process which gives rise to edges in the image. Provided that any a priori knowledge about the local edges to be extracted is unknown, it is necessary to select the scale (or support) of the edge operator which optimally adapts to the local scale of the edge in order to perform edge extraction correctly.

Most existing approaches to higher dimensional edge extraction have used the 1-D step or, respectively, the 1-D sigmoid edge profile as a model in an either implicit or explicit way (see e.g. [5], [6], [9]). However, the 1-D sigmoid edge model represents an ideally smooth 1-D intensity change and by generalizing it to

higher dimensions its scale cannot be always accurately determined. This can be easily seen for the case when a large scale operator has to be necessarily applied to a 2-D high-curvature contour undergoing a large Gaussian blurring: The large scale of the operator conflicts with the high curvature. As a consequence, only for the case of a linear replication of the 1-D sigmoid along the second orthogonal dimension a large scale operator can be safely applied as yet. A typical example of high curvature contours is a corner, and arbitrary Gaussian smoothing of its curve results in destroying its salient properties (see e.g. [10]).

In this paper, we consider the issue of optimal scale selection for circular edge extraction in the context of higher dimensional multiscale edge extraction and we focus on the principal way of how to analyze the effects of curvature as related to scale in multiscale edge extraction. First, based on a classification of higher dimensional edges according to local curvature, we exemplarily establish a 2-D circular edge model. Utilizing this model, we develop a theoretical framework for optimal scale selection and we analyze the effects of curvature as related to scale. Then, we present the results of a validation study of our optimal scale selection approach, where we investigate how well the experimental results obtained from application of the developed framework to 2-D synthetic images match the theoretical results. Note that we here deal with the 2-D case only, however, the basic approach can be potentially generalized to the higher dimensional case.

2 Towards Higher Dimensional Edge Models

We coarsely classify higher dimensional edges according to their local curvature into three types, i.e. *straight edges*, *circular edges*, and *corners*, while assuming a sigmoid-like profile. In more concrete terms, for a given radius R of a circular edge its corresponding curvature K is given by the reciprocal of the radius (i.e. $|K| = 1/R$), and the curvature is assumed to be constant. Furthermore, we assume edge points on an edge contour of descending curvature to form straight or straight-like edges and edge points on an edge contour of ascending curvature to represent corners or corner-like structures.

As a matter of fact, one can differently classify higher dimensional edges according to other alternative criteria. Our classification for establishing higher dimensional edge models is the first attempt to approach higher dimensional edge extraction theoretically in order to analyze the effects of curvature as related to scale in multiscale edge extraction, although our 2-D edge models based on this classification may not be sufficiently general to represent all edge types in real images. In this paper, we concentrate on the circular edge case.

2.1 Circular Edge Model

A unit circular edge of radius R is described by $\mathcal{H}(R^2 - x^2 - y^2)$, where $\mathcal{H}$ denotes the Heaviside function. Similar types of the circular edge model based upon the Heaviside function have been used for modeling curved edges with

constant curvature e.g. in [4]. The sigmoid unit circular edge with edge width t_E is represented by convolution of the Heaviside function with a Gaussian, i.e.

$$E_c(x,y;t_E) = \mathcal{H}(R^2-x^2-y^2) * G(x,y;t_E)$$
$$= R\int_{-1}^{1} G(x-R\cdot\gamma;t_E)\left(\Phi\left(y+R\sqrt{1-\gamma^2};t_E\right)-\Phi\left(y-R\sqrt{1-\gamma^2};t_E\right)\right)d\gamma,$$

where Φ is the normalized error integral function and the edge width t_E corresponds to the scale of edge. Unfortunately since the general analytical solution of $\int G\cdot\Phi$ is unknown ([4]), $E_c(x,y;t_E)$ cannot be determined analytically. However, we can transform $E_c(x,y;t_E)$ represented in Cartesian coordinates into polar coordinates without loss of generality since $\mathcal{H}(R^2-x^2-y^2)$ and $G(x,y;t_E)$ are rotationally symmetric in Cartesian coordinates.

2.2 The Gradient in Polar Coordinates

For a multiscale analysis, we derive the scale-space representation of a sigmoid circular edge, which we denote $L_{E_c}(x,y;t)$ and this is given by convolution with the Gaussian of variance t. For the further derivation, $L_{E_c}(x,y;t)$ in Cartesian coordinates must be transformed into $L_{E_c}(r;t)$ in polar coordinates ($r^2 = x^2 + y^2$):

$$L_{E_c}(r;t) = \mathcal{H}(R-r) * G(r;t_E+t) \quad (t_E, t>0), \tag{1}$$

where t_E and t, respectively, correspond to the edge width of a circular edge and the scale parameter, and $G(r;t_E+t) = \frac{1}{2\pi(t_E+t)}e^{-\frac{r^2}{2(t_E+t)}}$.

Considering the polar coordinates (r,θ), for any point $P=(x,y)$ in Cartesian coordinates we have

$$\begin{cases} x = r\cos\theta \\ y = r\sin\theta \end{cases}, \begin{cases} r = \sqrt{x^2+y^2} \\ \theta = \tan^{-1}\left(\frac{y}{x}\right) \end{cases}, \text{ and } \begin{cases} \frac{\partial r}{\partial x} = \frac{x}{\sqrt{x^2+y^2}} = \frac{r\cos\theta}{r} = \cos\theta \\ \frac{\partial r}{\partial y} = \frac{y}{\sqrt{x^2+y^2}} = \frac{r\sin\theta}{r} = \sin\theta \end{cases}.$$

Then, the gradient of $L_{E_c}(r;t)$ is given by

$$\nabla L_{E_c}(r;t) = \left(\frac{\partial L_{E_c}(r;t)}{\partial x}, \frac{\partial L_{E_c}(r;t)}{\partial y}\right)^T = \left(\frac{\partial L_{E_c}(r;t)}{\partial r}\cdot\cos\theta, \frac{\partial L_{E_c}(r;t)}{\partial r}\cdot\sin\theta\right)^T,$$

and the gradient magnitude of $L_{E_c}(r;t)$ is given by

$$|\nabla L_{E_c}(r;t)| = \sqrt{\left(\frac{\partial L_{E_c}(r;t)}{\partial r}\right)^2\cdot\cos^2\theta + \left(\frac{\partial L_{E_c}(r;t)}{\partial r}\right)^2\cdot\sin^2\theta} = \left|\frac{\partial L_{E_c}(r;t)}{\partial r}\right|.$$

In sum, we obtain

$$|\nabla L_{E_c}(r;t)| = \frac{R}{t_E+t}e^{-\frac{r^2+R^2}{2(t_E+t)}}I_1\left(\frac{R\cdot r}{t_E+t}\right) \tag{2}$$

(see Appendix for the detailed derivation), where I_1 denotes the modified Bessel function of integer order 1, which is a monotonously increasing function. Note that the modified Bessel function of integer order n is defined by $I_n(z) = \frac{1}{2\pi}\int_0^{2\pi} \cos(n\theta)e^{z\cos\theta}\, d\theta$ (cf. [1]).

3 Scale Selection in Circular Edge Extraction

Using the circular edge model in polar coordinates, we attempt to analyze the behavior of circular edges over scales for the purpose of selecting their optimal scale values. Let $M(t)$ be a response function of the gradient magnitude given in (2) at edges ($r = R$); that is, $M(t) = |\nabla L_{E_c}(R;t)|$. $M(t)$ is a monotonously decreasing function of t, which means that the edge operator response becomes weaker as the scale parameter increases, and thus $M(t)$ is not suitable for optimal scale selection.

On the other hand, by utilizing $M(t)$ we intend to find a response function from which an optimal scale (i.e. the edge width t_E) is uniquely selected. Although finding such a response function is quite difficult due to the complexity of $M(t)$, fortunately one can simplify $M(t)$ in a special case. Let $S(t)$ be a response function obtained from multiplying $M(t)$ with e^R as given by

$$S(t) = \frac{R}{t_E + t} e^{\frac{-R^2 + R(t_E+t)}{t_E+t}} I_1\left(\frac{R^2}{t_E + t}\right), \tag{3}$$

from which one can observe that, when $t_E + t = R$, $S(t)$ reduces to $I_1(R)$ (i.e. $S(t)|_{t_E+t=R} = \frac{R}{R}e^{\frac{-R^2+R^2}{R}} I_1(R) = I_1(R)$), which implies that $S(t)$ gives the response $I_1(R)$ when $t_E + t = R$. That is, the scale value satisfying $S(t) = I_1(R)$ corresponds to $t = R - t_E$. For a given R, $I_1(R)$ is known, from which one can uniquely obtain the value t satisfying $S(t)$=$I_1(R)$. The obtained value t, in turn, can be used to derive the optimal scale value t_E (i.e. $t_E = R - t$).

It is worth noting that there does not exist any t in the response of $S(t)$ satisfying $S(t)$=$I_1(R)$ where $R \leq t_E$. As a matter of fact, from a theoretical and practical viewpoint it is meaningless to consider the case for which the radius of a given circular edge is smaller than its edge width (see Sect. 4.1 for the unit of R, t, and t_E). Our theoretical derivation shows that $R \leq t_E$ corresponds to $t \leq 0$. We denote the relationship $R \leq t_E$ the *curvature-scale constraint*. This constraint can be used as a natural limit condition of curvature as related to the edge width for a given circular edge. Consequently, the optimal scale value for circular edges can be uniquely selected using the response function $S(t)$ given in (3) such that the optimal scale value of a given circular edge with the radius R is given by $t_E = R - t$, where t satisfies $S(t) = I_1(R)$.

4 Validation of the Optimal Scale Selection Approach

In this section, we validate the developed theoretical framework using synthetic images through investigating how well the experimental results obtained from

application of the developed framework to an image match the theoretical results. Through this validation study, i) we aim to check experimentally for the correctness of our theoretical derivation, ii) we demonstrate in practice the principal performance of optimal scale selection, and (iii) we can probe the limits for some extreme cases. Since the optimal scale value (i.e. the edge width) must be known a priori for our validation study, we use synthetic images and control the degree of edge width as well as the level of noise in the experiments. Note that the full range of experiments, e.g. by fine-sampling of the continuous parameter space, is beyond the scope of this paper and thus left open for future work.

4.1 Experimental Setting

For edge extraction, we use the discrete scale-space (DSS) kernel as well as its first-order odd-number-sized differencing kernel (i.e. $T_{\triangle_{\mathrm{odd}}}$) both of which are validated as best performing kernels in [7] and [8], and we employ the non-maxima suppression method by Canny [3].

We apply the developed framework for optimal scale selection to blurred noisy synthetic images and observe whether the theoretically expected scale is selected correctly. For a given synthetic image, we control the degree of edge width by convolving the image with the DSS kernel, the variance (t_E) of which varies from $\frac{1}{3}$ to $\frac{13}{3}$ (i.e. $t_E = \frac{k}{3}, k = 1, 2, \ldots, 13$) in our experiments. Given a blurred synthetic image, we add two different levels of Gaussian noise. We use three synthetic images C_i representing three different types of a circular edge (see Fig. 1). For a given degree of edge width k, let us denote $\tau(k)$ a selected scale value resulting from the application of the developed framework for optimal scale selection to C_i of Fig. 1. With respect to $\tau(k)$, we consider the mean ($\overline{\tau}(k)$) and the standard deviation ($\tau_\sigma(k)$) of $\tau(k)$ along the edge contour. According to the optimal scale selection scheme theoretically derived in the previous section, $\frac{\tau(k)}{3} = R - \frac{k}{3}$ viz. $\tau(k) = 3R - k$ must hold.

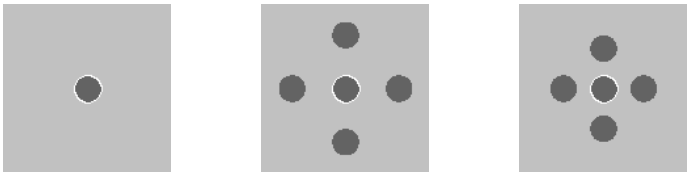

Fig. 1. Synthetic images C1 (left), C2 (middle), and C3 (right) representing three different types of circular edge. The radius of a circle is $R = 10$ (occupying 10 pixels) in our experiment. The in-between-distance of neighboring circles in C2 corresponds to the diameter of the given circle, while that in C3 corresponds to the radius of the given circle. The white contour marks the edge loci to be observed.

4.2 Experimental Results and Assessment

Fig. 2 gives a graphical illustration of the experimental results for C1, C2, and C3 in terms of $\{\overline{\tau}, \tau_\sigma\}$ compared with the theoretical result. One can notice several remarkable aspects from Fig. 2. First, the obtained experimental results are in general very close to the theoretical results. The slight deviation of the experimental results from the theoretical ones may be rightfully assumed to be caused by an inevitable gap between a well-founded continuous theory and the implemented discrete case. In other words, even though the circular edge contours of the synthetic images used in our experiment were obtained from the mathematical equation of a circle, strictly speaking, they are not perfectly circular in a digital image. Second, the experimental results are affected by noise only little. This is because that the radius value of a circular edge plays a decisive role in the developed framework for optimal scale selection, where the selected optimal scale value mainly depends on the radius value, and thus the level of noise has less influence. Moreover, the degree of the in-between-distance has little effect on the result of optimal scale selection, where 'little' is only valid with respect to our experiment regarding the condition that the in-between-distance of neighboring circles should be larger than 10 pixels (see Fig. 1).

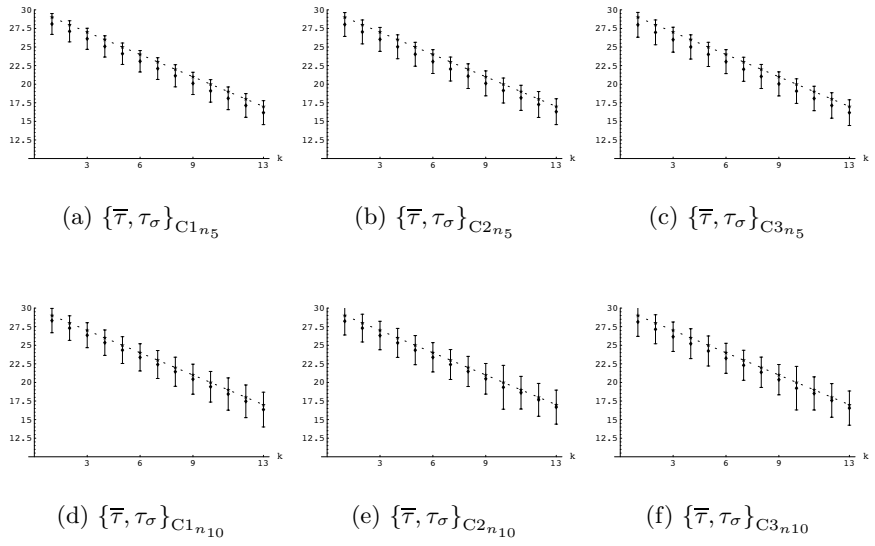

(a) $\{\overline{\tau}, \tau_\sigma\}_{\mathrm{C1}n_5}$ (b) $\{\overline{\tau}, \tau_\sigma\}_{\mathrm{C2}n_5}$ (c) $\{\overline{\tau}, \tau_\sigma\}_{\mathrm{C3}n_5}$

(d) $\{\overline{\tau}, \tau_\sigma\}_{\mathrm{C1}n_{10}}$ (e) $\{\overline{\tau}, \tau_\sigma\}_{\mathrm{C2}n_{10}}$ (f) $\{\overline{\tau}, \tau_\sigma\}_{\mathrm{C3}n10}$

Fig. 2. Graphical illustration of experimental results for C1, C2, and C3 compared with the theoretical result. Each column differs in the type of circular edge and each row differs in the level of noise (n_5 and n_{10} denote weak noise and strong noise, respectively). '$\cdots\bigstar\cdots$' corresponds to the theoretical result (i.e. $\tau(k) = 3R - k$ for $R = 10$; see Sect. 4.1), while '⧫' with error bar represents the experimental result.

5 Summary and Conclusions

In this paper, we proposed a theoretical framework for optimal scale selection in circular edge extraction. We established a 2-D circular edge model based on a classification of 2-D edges according to local curvature. By transforming the circular edge model from Cartesian coordinates for which the analytical solution is unknown into polar coordinates, we were able to analyze the effects of curvature as related to scale, which is a novel approach based on a careful mathematical derivation. Moreover, we presented the results of our validation study in which we investigated how well the experimental results obtained from application of the developed framework to 2-D synthetic images match the theoretical results. Our validation study shows that the experimental results are generally close to the theoretical results on the whole. Future work will include an investigation of the 3-D case. Also, it is necessary to consider how robustly and accurately edge extraction based on our developed framework performs in real-world images.

Appendix: Transformation of the circular edge model from Cartesian coordinates into polar coordinates

Provided that $f(r)$ and $g(r)$ are both rotationally symmetric, convolution of $f(r)$ with $g(r)$ in polar coordinates is defined ([2, p. 339]) by

$$f(r) * g(r) = \int_0^{\infty} \int_0^{2\pi} f(r')g(s)r' \, dr' \, d\theta' \quad \left(s^2 = r^2 + r'^2 - 2rr' \cos\theta'\right),$$

according to which (1) is derived as (denoting $T = t_E + t$)

$$L(r;t) = \mathcal{H}(R-r) * G(r;T) = \int_0^{\infty} \int_0^{2\pi} r'\mathcal{H}(R-r')\frac{1}{2\pi T} e^{-\frac{r'^2+r^2-2rr'\cos\theta'}{2T}} dr' d\theta'$$

$$= \frac{1}{T}\int_0^R r' e^{-\frac{r'^2+r^2}{2T}} \int_0^{2\pi} \frac{1}{2\pi} e^{\frac{rr'\cos\theta'}{T}} \, d\theta' \, dr' = \frac{1}{T}\int_0^R r' e^{-\frac{r'^2+r^2}{2T}} I_0\left(\frac{rr'}{T}\right) \, dr',$$

where $I_0(\cdot)$ is the modified Bessel function of integer order 0 (see Sect.2.2 for the definition). Then $\frac{dL(r;t)}{dr} = \frac{1}{T}\int_0^R r' \frac{d}{dr}\left(e^{-\frac{r'^2+r^2}{2T}} I_0(\frac{rr'}{T})\right) dr'$ is derived as

$$\frac{1}{T}\int_0^R \left[\frac{r'^2}{T} e^{-\frac{r'^2+r^2}{2T}} I_1\left(\frac{rr'}{T}\right) - \frac{rr'}{T} e^{-\frac{r'^2+r^2}{2T}} I_0\left(\frac{rr'}{T}\right)\right] dr' \quad (\text{cf. } I_0'(z) = I_1(z))$$

$$= \frac{1}{T}\int_0^R \left[-r' \frac{d\left(e^{-\frac{r'^2+r^2}{2T}}\right)}{dr'} I_1\left(\frac{rr'}{T}\right) - e^{-\frac{r'^2+r^2}{2T}} \underbrace{\frac{rr'}{T} I_0\left(\frac{rr'}{T}\right)}_{**}\right] dr'.$$

Using the recurrence relations of the Bessel functions $I_n'(z) = \frac{I_{n-1}(z)+I_{n+1}(z)}{2}$ and $I_n(z) = \frac{z}{2n} I_{n-1}(z) - \frac{z}{2n} I_{n+1}(z)$ (see [1] for details), the above term $\frac{rr'}{T} I_0\left(\frac{rr'}{T}\right)$

denoted by '**' corresponds to

$$\frac{rr' I_0\left(\frac{rr'}{T}\right) + rr' I_0\left(\frac{rr'}{T}\right)}{2T} = \frac{rr'}{2T} I_0\left(\frac{rr'}{T}\right) + I_1\left(\frac{rr'}{T}\right) + \frac{rr'}{2T} I_2\left(\frac{rr'}{T}\right)$$
$$= \frac{I_0\left(\frac{rr'}{T}\right) + I_2\left(\frac{rr'}{T}\right)}{2} \frac{rr'}{T} + I_1\left(\frac{rr'}{T}\right) = r' \frac{d\left(I_1\left(\frac{rr'}{T}\right)\right)}{dr'} + I_1\left(\frac{rr'}{T}\right) \frac{dr'}{dr'}.$$

As a consequence, $\frac{dL(r;t)}{dr}$ is derived as

$$\frac{1}{T} \int_0^R \left[-r' \frac{d\left(e^{-\frac{r'^2+r^2}{2T}}\right)}{dr'} I_1\left(\frac{rr'}{T}\right) - e^{-\frac{r'^2+r^2}{2T}} \left(r' \frac{d\left(I_1\left(\frac{rr'}{T}\right)\right)}{dr'} + I_1\left(\frac{rr'}{T}\right) \frac{dr'}{dr'} \right) \right] dr'$$
$$= \frac{1}{T} \int_0^R - \frac{d\left(r' e^{-\frac{r'^2+r^2}{2T}} I_1\left(\frac{rr'}{T}\right)\right)}{dr'} \, dr' = -\frac{R}{T} e^{-\frac{R^2+r^2}{2T}} I_1\left(\frac{Rr}{T}\right).$$

Acknowledgement

The financial support by DAAD (German Academic Exchange Service) to the first author is greatly acknowledged. The authors thank Dr. Ullrich Köthe for his valuable help in deriving (2).

References

1. M. Abramowitz and I. A. Stegun, *Handbook of Mathematical Functions*, Dover Publisher, the 9th edition, 1972
2. R. N. Bracewell, *The Fourier Transform and Its Applications*, McGraw-Hill, the 3rd edition, 2000
3. J. F. Canny, "A Computational Approach to Edge Detection", *IEEE Trans. on Pattern Analysis and Machine Intelligence* (PAMI), Vol. 8(6), pp. 679-698, 1986
4. C. Drewniok, *Objektlokalisation durch Adaption parametrischer Grauwertmodelle und ihre Anwendung in der Luftbildauswertung*, Dissertation, Uni. Hamburg, 1999
5. J. H. Elder and S. W. Zucker, "Local Scale Control for Edge Detection and Blur Estimation", PAMI Vol. 20(7), pp. 699-716, 1998
6. A. F. Korn, "Toward a Symbolic Representation of Intensity Changes in Images", PAMI Vol. 10(5), pp. 610-625, 1988
7. J. Y. Lim, *Discrete Scale-Space Formulation and Multiscale Edge Extraction toward Higher Dimensions*, Dissertation (to be published), Uni. Hamburg, 2003
8. J. Y. Lim and H. S. Stiehl, "A Generalized Discrete Scale-Space Formulation for 2-D and 3-D Signals", *The 4th Int. Conf. on Scale-Space Theories in Computer Vision*, Skye/Scotland, 10–12 June, 2003
9. T. Lindeberg, "Edge Detection and Ridge Detection with Automatic Scale Selection", *Int. Journal of Computer Vision*, Vol. 3(2), pp. 117-154, 1998
10. K. Rohr, "Recognizing Corners by Fitting Parametric Models", *Int. Journal of Computer Vision*, Vol. 9(3), pp. 213-230, 1992
11. J. Sporring, M. Nielsen, L. M. J. Florack P. Johansen, *Gaussian Scale-Space Theory*, Kluwer Academic Publishers, 1997